Journal of Molecular Spectroscopy 318 (2015) 84–90

Contents lists available at ScienceDirect

Journal of Molecular Spectroscopy

journal homepage: www.elsevier.com/locate/jms

A variationally calculated room temperature line-list for H_2O_2

Ahmed F. Al-Refaie [a], Roman I. Ovsyannikov [b], Oleg L. Polyansky [a], Sergei N. Yurchenko [a], Jonathan Tennyson [a,*]

[a] Department of Physics and Astronomy, University College London, London WC1E 6BT, UK
[b] Institute of Applied Physics, Russian Academy of Sciences, Ulyanov Street 46, Nizhny Novgorod 603950, Russia

ARTICLE INFO

Article history:
Received 2 September 2015
In revised form 4 October 2015
Accepted 5 October 2015
Available online 8 October 2015

Keywords:
Hydrogen peroxide
Dipole moment
Infrared
Transition dipole
Vibration
HOOH
Intensity
Variational calculations

ABSTRACT

A room temperature line list for hydrogen peroxide is computed using a high level *ab initio* potential energy surface by Małyszek and Koput (2013) with a small adjustment of the equilibrium geometry and height of the torsional barrier and a new *ab initio* dipole moment surface (CCSD(T)-f12b/aug-cc-pv(T+d)Z). In order to improve further the *ab initio* accuracy, the vibrational band centers were shifted to match experimental values when available. The line list covers the wavenumber region up to 8000 cm^{-1} with the rotational excitations $J \leqslant 40$. Room temperatures synthetic spectra of H_2O_2 are generated and compared to the spectra from the HITRAN and PNNL-IR databases showing good agrement.

1. Introduction

Hydrogen peroxide is a trace species in Earth [1–3] atmospheric chemistry and plays a role in stratospheric ozone production. There have been multiple detections of H_2O_2 in the Martian atmosphere [4–7], where it is possibly formed by triboelectricity in dust devils and dust storms [6] and it may well act as an agent in the oxidization of the Martian surface. A recent detection in the interstellar medium [8] gives insight to the formation of water in space. Finally H_2O_2 has been detected in the atmosphere of Europa [9] in the 3.5 μm (≈2587 cm^{-1}) region.

Hydrogen peroxide is an asymmetric prolate rotor molecule. Its most interesting characteristic is that it is the simplest molecule that exhibits internal (torsional) rotation. This gives it a double-minimum in its torsional potential as well as two alignments of the O–H bonds: *cis* and *trans*. The torsional mode therefore contains four 'sub-levels' for each excitation and requires an additional internal-rotation quantum number ($\tau = 1, 2, 3, 4$) [10] to properly characterize it. It also only exhibits c-type transitions which consequently means it has no pure rotational transitions. H_2O_2 has six vibrational modes: ν_1 and ν_5 represent the symmetric and asymmetric O–H stretching respectively, ν_3 and ν_6 represent the O–H bending respectively, ν_2 represents the O–O stretch and the ν_4 mode represents the torsional excitation and is commonly represented in literature as *n*.

The HITRAN 2012 database [11] only contains transitions for hydrogen peroxide below 1800 cm^{-1}. This region covers the torsional, O–H bending modes and O–O stretch but misses the O–H stretches at the 3750 cm^{-1} region. Only a few studies deal with spectra of H_2O_2 in the mid-infrared and near-infrared [12–14] regions. Available experimental studies mostly concern torsional rovibrational transitions involving the ground and excited states [15], and the ν_3 [16] and ν_6 [14] vibrational modes. Whilst there are ample data available in the literature for the torsional and bending bands, the fundamental stretching modes are more difficult to obtain accurate term values for. The O–H stretching modes, ν_1 and ν_5, in particular have been especially problematic. The separation between the two bands is about 8–10 cm^{-1} and torsional splitting from the double minimum of the potential gives rise to doubling [17] in the form of 'quasi'-degenerate states [18] that are difficult to resolve accurately. Olsen et al. [15] give an estimate of 3610–3618 cm^{-1} for ν_5 and 3601–3617 cm^{-1} for ν_1 whilst a Raman study gives a lower value of 3607 cm^{-1} [17] for the ν_1 band-center but determining the accuracy to better than 0.1 cm^{-1} is difficult. A theoretical line-list may provide a way of characterizing the confusing spectra of H_2O_2 above 1800 cm^{-1} but so far none have been produced.

* Corresponding author.
E-mail address: j.tennyson@ucl.ac.uk (J. Tennyson).

http://dx.doi.org/10.1016/j.jms.2015.10.004
0022-2852/

In this work we present a room temperature line list generated using the variational approach TROVE [19,20] based on a high quality *ab initio* potential energy [21,22] and new dipole moment surfaces.

2. Method

The accuracy of the line positions is determined by the quality of the PES. The PES is based of the high-accuracy *ab initio* calculations of Małyszek and Koput [21]. The PES was computed using the CCSD(T)-F12 method with parts of the PES utilizing aug-cc-pV7Z basis-sets. These calculations can be considered state-of-the-art for this problem. We include the small adjustment to the *ab initio* equilibrium geometry and height of the torsional barrier proposed by Polyansky et al. [22]. The PES boasts a root-mean-squares (rms) difference of 0.02 cm^{-1} for rotational levels up to $J = 35$ within low-lying vibrational states [22].

The rovibrational energies were calculated using the TROVE [19] computer suite. TROVE is a variational nuclear-motion solver and can be employed in all steps of line-list production for molecules of arbitrary structure. It has been successful to produce hot line lists for CH_4 [23], PH_3 [24], H_2CO [25] and room temperature ones for PH_3 [26] and SO_3 [27]. TROVE was also used to simulate a room temperature spectrum for another non-rigid, chain molecule HSOH based on a high level *ab initio* potential energy and dipole moment surfaces [28,29].

Within TROVE, the nuclear-motion Hamiltonian is represented as an expansion around a reference configuration where the bond lengths for the O–O bond (R), the O–H_1 bond (r_1), the O–H_2 bond (r_2) and the bond angles for O–H_1 (θ_1) and O–H_2 (θ_2) are frozen at their equilibrium and the torsional angle τ varies on a grid of 10,000 values ranging from 0° to 720°. The internal co-ordinates are described in Fig. 1.

TROVE utilizes an approximate kinetic energy operator (KEO). Comparisons with exact KEO codes such as WAVR4 [30] show TROVE converging just as well [22] whilst being less computationally demanding. Convergence is obtained for expansion orders between 6 and 8 [19].

Here, the kinetic energy is expanded around the reference geometry in terms of five linearized co-ordinates of the form:

$$\zeta_i = x_i^l - x_i^e, \tag{1}$$

where x_i^l and x_i^e represents linearized version and equilibrium geometry of the bond lengths and angles respectively. Here, $i = 1$, $i = 2$, $i = 3$, $i = 4$ and $i = 5$ represent R, r_1, r_2, θ_1 and θ_2 respectively and $i = 6$ is the sixth co-ordinate, $\zeta_6 = \tau$. The potential is also expanded in terms of the Morse-type coordinates $\zeta_1 = 1 - \exp(-a_i\zeta_i)$ (a_i are parameters, $i = 1,2,3$) for the stretches and the displacements or ζ_4 and ζ_5 for the two bends. For this work the kinetic energy expansion order is 6 and the potential expansion order is 8.

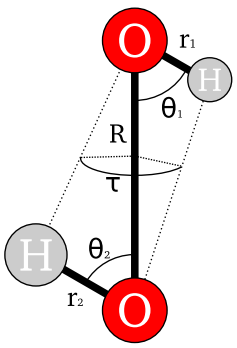

Fig. 1. The internal co-ordinates of HOOH.

A symmetry-adapted basis-set is constructed by a multi-step contraction scheme that is truncated via polyad number $P_{max} = 42$ [22]. The primitive vibrational basis-set is constructed by solving the 1D Schrodinger equation for each basis-function $\phi_{v_i}(\zeta_i)(i = 1,2,\ldots,6)$ associated with the vibrational quantum number v_i via the Numerov–Cooley method [31,32] for each mode allowed by the polyad P:

$$P = 4v_1 + 8(v_2 + v_3 + v_4 + v_5) + v_6 \leqslant P_{max}. \tag{2}$$

The six dimensional co-ordinate space is then divided into four reduced subspaces: (ζ_1), (ζ_2,ζ_3), (ζ_4,ζ_5) and (ζ_6) based on symmetry. The reduced Hamiltonian is solved using the primitives ϕ_{v_i} as basis-functions to obtain the contracted vibrational basis-functions $\Phi_{n_1}(\zeta_1)$, $\Phi_{n_2}(\zeta_2,\zeta_3)$, $\Phi_{n_3}(\zeta_4,\zeta_5)$ and $\Phi_{n_4}(\zeta_6)$. These basis-functions are then symmetrised according to the $\mathcal{D}_{2h}$(M) Molecular Group symmetry [33] and the final vibrational basis-set is formed from the product of the four contracted basis-functions which are truncated via Eq. (2) and symmetrized again. The general form of the Hamiltonian operator is:

$$H = H_{vib} + \frac{1}{2}\sum_{\alpha\beta} J_\alpha G_{\alpha\beta} J_\beta + \frac{1}{2}\sum_{\alpha\lambda}(p_\lambda G_{\lambda\alpha} + G_{\alpha\lambda}p_\lambda)J_\alpha, \tag{3}$$

where J_α and p_λ are the rotational and vibrational momentum operators respectively and H_{vib} is the pure vibrational ($J = 0$) Hamiltonian given as:

$$H_{vib} = \frac{1}{2}\sum_{\lambda\mu} p_\lambda G_{\lambda\mu} p_\mu + V + U, \tag{4}$$

where $G_{\alpha\beta}$ are kinetic energy factors, U is a pseudo-potential [19] and V is the molecular potential energy. The contracted Hamiltonian is solved up to an energy eigenvalue threshold of 24,000 cm^{-1}. A final contraction step can be performed by solving the $J = 0$ problem given by Eq. (4) and replacing the bulky primitive vibrational basis-sets with the more compact $J = 0$ wavefunctions. This has the added benefit of making the computation of the Hamiltonian matrix elements for $J > 0$ more efficient as the H_{vib} contribution becomes:

$$\langle \Psi^\Gamma_{J=0,i} | H_{vib} | \Psi^\Gamma_{J=0,i'} \rangle = E_i \delta_{i,i'}\ , \tag{5}$$

Table 1
Experimental [15,16,36,37] band centers used in the empirical shift.

v_1	v_2	v_3	v_4	v_5	v_6	τ	Symmetry	Ab initio (cm^{-1})	Shifted/Obs (cm^{-1})
0	0	0	0	0	0	4	A_u	11.312	11.437
0	0	0	0	0	0	3	B_{2u}	11.312	11.437
0	0	0	1	0	0	1	A_g	255.529	254.55
0	0	0	1	0	0	2	B_{2g}	255.532	254.55
0	0	0	1	0	0	4	A_u	371.589	370.893
0	0	0	1	0	0	3	B_{2u}	371.590	370.893
0	0	0	2	0	0	1	A_g	570.809	569.743
0	0	0	2	0	0	2	B_{2g}	570.818	569.743
0	0	0	2	0	0	4	A_u	777.432	776.1221
0	0	0	2	0	0	3	B_{2u}	777.458	776.1148
0	0	1	0	0	0	1	A_g	865.539	865.939
0	0	1	0	0	0	2	B_{2g}	865.539	865.939
0	0	1	0	0	0	4	A_u	877.470	877.934
0	0	1	0	0	0	3	B_{2u}	877.470	877.934
0	0	0	3	0	0	1	A_g	1002.666	1000.882
0	0	0	3	0	0	2	B_{2g}	1002.869	1000.930
0	0	0	0	0	1	1	B_{1u}	1265.003	1264.583
0	0	0	0	0	1	3	B_{1g}	1285.879	1285.121
0	0	0	1	0	1	1	B_{1u}	1506.164	1504.872
0	0	0	1	0	0	3	B_{1g}	1649.977	1648.367
0	0	0	2	0	1	1	B_{1u}	1855.823	1853.634
0	0	0	2	0	1	3	B_{1g}	2075.366	2072.404

where $\Psi^{\Gamma}_{J=0,i}$ is the symmetrized wavefunction of a particular state i obtained from Eq. (4). The vibrational contribution is both diagonal and simply the eigenvalue of $\Psi^{\Gamma}_{J=0,i}$. Additionally, experimental band centers can be substituted instead of the eigenvalues, this 'shifts' the band center onto the experimental value and allows further rotational excitations to be computed around the experimental band centers. Here the $J = 0$ wavefunctions with eigenvalues up to 8000 cm^{-1} are utilized further reducing the size of the Hamiltonian. The original primitive basis-set was of size 2,789,400, this was reduced to 23,078 in the contracted and finally to 2875 using the $J = 0$ 'form'. A more detailed explanation of this methodology is given by Yurchenko et al. [34].

Using these symmetrized wavefunctions also has the benefit that the Hamiltonian matrix is factorized into independent blocks according to the $\mathcal{D}_{2h}(M)$ symmetry. $\mathcal{D}_{2h}(M)$ is isomorphic to the $C^{+}_{2h}(M)$ symmetry group which best describes the torsional splitting caused by the *cis* and *trans* tunneling [35]. The irreducible representations of this group are A_g, A_u, B_{1g}, B_{1u}, B_{2g}, B_{2u}, B_{3g} and B_{3u}. However, the states corresponding to B_{2g}, B_{2u}, B_{3g} and B_{3u} have zero statistical weight and therefore their matrix blocks are not constructed and diagonalized for $J > 0$. It is usual to describe the H_2O_2 torsional modes using the notation (n, τ), where n is the excitation of the torsional mode. The excitations of the torsional (ν_4/n) mode are represented by A_g, A_u, B_{2g} or B_{2u} symmetry which correspond to the quanta $\tau = 1$, $\tau = 4$, $\tau = 2$ and $\tau = 3$, respectively. This needs to be taken into account when manipulating the band-centers as it requires modifying the B_{2g} or B_{2u} eigenvalues in order to properly represent the splitting at higher J. Table 1 lists all the band-centers that were utilized in the empirical shifts together with the *ab initio* values before the shift.

The τ quantum number can be preserved in the quantum number assignment in TROVE by utilizing the following form:

$$\nu_4 = 4n + i, \tag{6}$$

where n is the excitation and i is the symmetry where $i = 0, 1, 2, 3$ is A_g, B_{2g}, B_{2u} and A_u, respectively. Integer quantum numbers n and τ can be simply retrieved:

$$\tau = (\nu_4 \bmod 4) + 1, \quad n = \left\lfloor \frac{\nu_4}{4} \right\rfloor. \tag{7}$$

The final line-list format will extract both numbers and utilize n as the value for ν_4 and include a separate τ quantum number which should not be confused with the commonly used rotational parity symbol $\tau_{rot} = \pm$ or with the torsional angle τ (see below). For this line-list, the Hamiltonian matrices up to the limit of $J = 40$ are constructed and diagonalized using the $J = 0$ contracted basis set for all eigenvalues and eigenvectors but only eigenvectors up to 8000 cm^{-1} are stored and used for producing the transitions.

2.1. Dipole moment surface and intensities

An electric dipole moment surface (DMS) is required to calculate the absolute intensities for each transition. An *ab initio* DMS was computed at the CCSD(T)-f12b/aug-cc-pV(T+d)Z [38] level of theory in the frozen-core approximation using CCSD(T) [39] on a grid of 50,000 geometries in conjunction with the finite electric field method and field of 0.005 a.u. We expect this DMS to be of adequate quality, as this level of theory is known to yield accurate intensities (see e.g., review [40]).

The $\mathcal{D}_{2h}(M)$ symmetry-adapted projections of the dipole moment Cartesian components μ_x, μ_y, and μ_z are given in the analytical representations with each component expanded in Taylor series (312 parameters in total) in terms of internal coordinates around the equilibrium configuration using a molecular-fixed axis system as follows. The z axis is aligned along the O–O bond, and

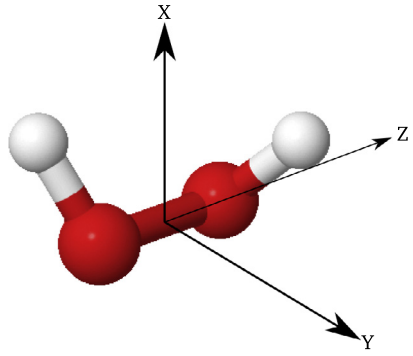

Fig. 2. The principal axis for HOOH used in the DMS expansion.

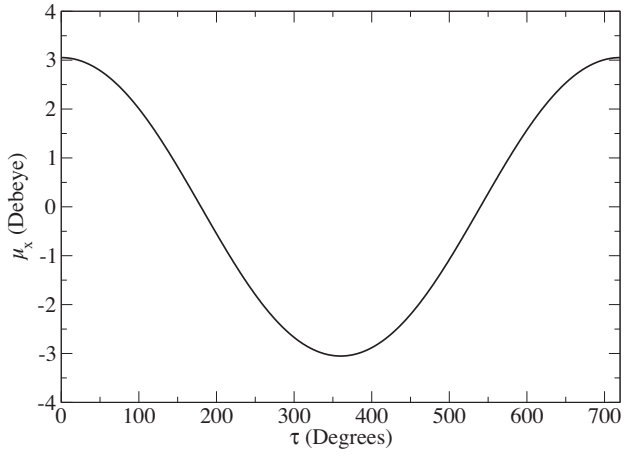

Fig. 3. The μ_x dipole moment component for H_2O_2, computed at the torsional geometries shown.

Table 2
Absolute values of experimental [13] and *ab initio* transition moments, in debye, for $(n', \tau = 1) \leftrightarrow (n'', \tau = 3)$.

n'	n''	Calc	Obs	(Obs-Calc)/Obs (%)
0	0	1.5683	1.5723	0.25
0	1	0.3332	0.3413	−2.40
1	0	0.6031	0.6136	−1.72
1	1	1.1664	1.1751	0.74
2	1	1.1664	1.1628	0.31
2	2	1.2638	1.2825	1.46
3	2	1.3276	1.3535	−1.91

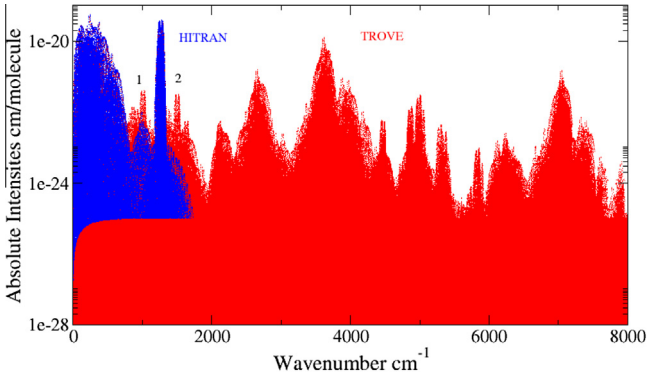

Fig. 4. Overview of our synthetic spectrum at $T = 296$ K against HITRAN [11].

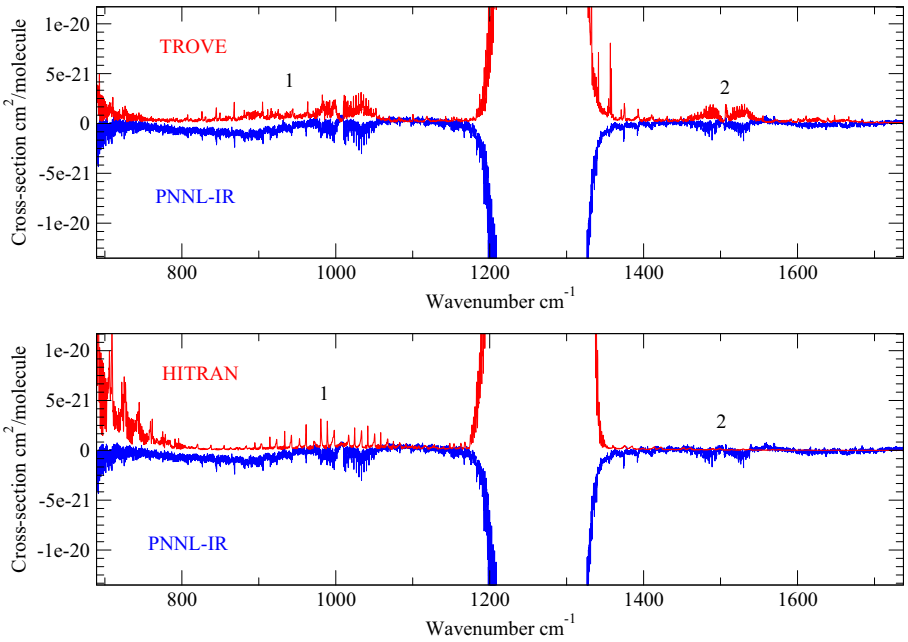

Fig. 5. Cross-section comparison of the room temperature line-list against experimental PNNL-IR [45] data at the ν_1 and ν_5 band at 323.15 K with HWHM = 0.3120 cm^{-1}.

the x axis lies in the plane bisecting the two O–O–H planes (i.e. planes containing the O–O and O–H bonds). The y axis is oriented such that the xyz axis system is right-handed. This xyz axes is not exactly but close to the principal axis system shown in Fig. 2. With the chosen axes, the x, y, and z components of the dipole moment span the B_{1u}, B_{3u}, and B_{2u} representations, respectively. The three electronically averaged dipole components are represented by the following analytical functions:

$$\bar{\mu}_x = \cos(\tau/2) \sum_{i_1,i_2,\ldots,i_6} \mu^{(x)}_{i_1,i_2,\ldots,i_6} \xi_1^{i_1} \xi_2^{i_2} \xi_3^{i_3} \xi_4^{i_4} \xi_5^{i_5} \xi_6^{i_6}, \quad (8)$$

$$\bar{\mu}_y = \sin(\tau/2) \sum_{i_1,i_2,\ldots,i_6} \mu^{(y)}_{i_1,i_2,\ldots,i_6} \xi_1^{i_1} \xi_2^{i_2} \xi_3^{i_3} \xi_4^{i_4} \xi_5^{i_5} \xi_6^{i_6}, \quad (9)$$

$$\bar{\mu}_z = \sum_{i_1,i_2,\ldots,i_6} \mu^{(z)}_{i_1,i_2,\ldots,i_6} \xi_1^{i_1} \xi_2^{i_2} \xi_3^{i_3} \xi_4^{i_4} \xi_5^{i_5} \xi_6^{i_6}, \quad (10)$$

where

$$\xi_1 = \Delta R e^{-(\Delta R)^2}, \quad (11)$$

$$\xi_2 = \Delta r_1 e^{-(\Delta r_1)^2}, \quad (12)$$

$$\xi_3 = \Delta r_2 e^{-(\Delta r_2)^2}, \quad (13)$$

$$\xi_4 = \Delta\theta_1, \quad (14)$$

$$\xi_5 = \Delta\theta_2, \quad (15)$$

$$\xi_6 = \cos\tau. \quad (16)$$

The expansion parameters of the x, y and z components of the dipole obey the following permutation rules:

$$\mu^{(x)}_{i_1,i_2,i_3,i_4,i_5,i_6} = \mu^{(x)}_{i_1,i_3,i_2,i_5,i_4,i_6}, \quad (17)$$

$$\mu^{(y)}_{i_1,i_2,i_3,i_4,i_5,i_6} = -\mu^{(y)}_{i_1,i_3,i_2,i_5,i_4,i_6}, \quad (18)$$

$$\mu^{(z)}_{i_1,i_2,i_3,i_4,i_5,i_6} = -\mu^{(z)}_{i_1,i_3,i_2,i_5,i_4,i_6}, \quad (19)$$

corresponding to the permutation of the two hydrogen atoms and therefore $\mu^{(\alpha)}_{0,0,0,0,0,i_6} = 0$ ($\alpha = y,z$) for any i_6. The dependance of μ_x component against the torsional angle is shown in Fig. 3.

The 130, 90, and 92 symmetrically independent expansion parameters $\mu^{(\alpha)}_{i_1,i_2,i_3,i_4,i_5,i_6}$ ($\alpha = x,y,z$) were obtained in a least-squares fit to the $3 \times 20{,}842$ *ab initio* dipole moment values

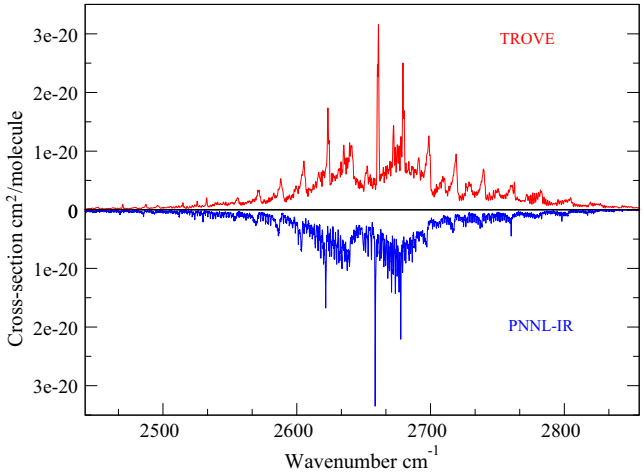

Fig. 6. Cross-section comparison of the room temperature line-list against experimental PNNL-IR [45] data at 323.15 K with HWHM = 0.3120 cm^{-1}.

(corresponding to energies below hc 12,000 cm^{-1}) with the rms error of 0.0013, 0.0002, and 0.0010 D, respectively.[1] The resulting DMS parameters are given in the Supplementary material.

In TROVE the *ab initio* DMS is re-expanded around the non-rigid reference configuration in terms of the ζ_i ($i = 1 \ldots 5$) variables as described above, using the numerical finite differences method [19]. At some torsional values close to $\tau = 360^\circ$ and $\tau = 720^\circ$ the finite differences produce discontinuities, which lead to meaningless values of the dipole expansion parameters $\mu_{i,j,k}(\tau)$ for a number of grid points. These points are treated as outliers and replaced by interpolated values. Additionally as the expansion is not an exact representation of the μ_α dipole component it may display artificial asymmetry. This is resolved by computing μ_α for torsional geometries up to $\tau = 360^\circ$ and then mirroring the values up to $\tau = 720^\circ$.

[1] 1 D = 3.33564×10^{-30} C m.

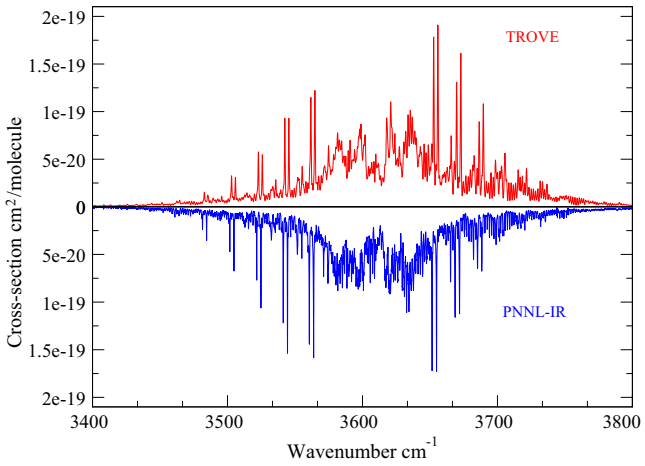

Fig. 7. Cross-section comparison of the room temperature line-list against experimental PNNL-IR [45] data at the ν_1 and ν_5 band at 323.15 K with HWHM = 0.3120 cm^{-1}.

Vibrational transition moment are computed as:

$$\mu_{if} = \sqrt{\sum_{A=x,y,z} |\langle \Psi^{\Gamma}_{J=0,i} | \bar{\mu}_A | \Psi^{\Gamma}_{J=0,f} \rangle|^2}. \tag{20}$$

Our vibrationally averaged moment for the ground vibrational state is 1.5683 D and compares well with measured of 1.5728 D [41]. This is very different from the equilibrium value of the *ab initio* dipole moment $\bar{\mu}^{e}_{x} = 1.738$ D (at $R = 1.4554$ Å, $r_1 = r_2 = 0.96257$ Å, $\theta_1 = \theta_2 = 101.083^{\circ}$), showing the strong non-rigid character of the H_2O_2 dipole moment.

Information on transition moments for H_2O_2 is limited; Table 2 compares available experimentally derived values at different torsional excitations from experiment [13]. Our calculated values reproduce the experimental with a maximum deviation of 2.4%. Some papers report effective transition dipole moments as a torsional expansion in terms of τ, e.g. $\phi_z \cos\tau$ (ϕ_z is a parameter) [13] which are difficult to compare to our fully averaged transition dipoles.

Using the DMS and eigenvectors obtained from diagonalization, the linestrengths for each transition can be computed providing they satisfy the selection rules:

$$J' - J'' = 0, \ \pm 1, \ J' + J'' \neq 0, \tag{21}$$

$$A_g \leftrightarrow A_u, B_{1g} \leftrightarrow B_{1u}, \tag{22}$$

and the B_{2g}, B_{2u}, B_{3g} and B_{3u} are forbidden due to their zero nuclear statistical weights. The Einstein-*A* coefficient for a particular transition from the *initial* state *i* to the *final* state *f* is given by:

$$A_{if} = \frac{64 \times 10^{-36} \pi^4 \tilde{\nu}^3_{if}}{3h} (2J_i + 1) \sum_{A=X,Y,Z} |\langle \Psi^f | \bar{\mu}_A | \Psi^i \rangle|^2, \tag{23}$$

where J_i is the rotational quantum number for the initial state, h is Planck's constant, $\tilde{\nu}_{if}$ is the transition frequency ($hc\,\tilde{\nu}_{if} = E_f - E_i$), Ψ^f and Ψ^i represent the eigenfunctions of the final and initial states respectively, $\bar{\mu}_A$ is the electronically averaged component of the dipole moment along the space-fixed axis $A = X, Y, Z$ (see also Yurchenko et al. [42]). From this the absolute absorption intensity is determined by:

$$I(f \leftarrow i) = \frac{A_{if}}{8\pi c} g_{\rm ns} (2J_f + 1) \frac{\exp\left(-\frac{E_i}{kT}\right)}{Q\,\tilde{\nu}^2_{if}} \left[1 - \exp\left(\frac{-hc\tilde{\nu}_{if}}{kT}\right)\right], \tag{24}$$

where k is the Boltzmann constant, T the absolute temperature and $g_{\rm ns}$ is the nuclear spin statistical weight factor. Q, the partition function, is given by:

$$Q = \sum_i g_i \exp\left(\frac{-E_i}{kT}\right), \tag{25}$$

where g_i is the degeneracy of a particular state i with energy E_i. For H_2O_2, g_i is $g_{\rm ns}(2J_i + 1)$ with $g_{\rm ns} = 1$ for A_g and A_u, $g_{\rm ns} = 3$ for B_{1g} and B_{1u} and $g_{\rm ns} = 0$ for the B_{2g}, B_{2u}, B_{3g} and B_{3u} symmetries. The transitions were computed using the energy limits *hc* 4000 and *hc* 8000 cm^{-1} for the lower and upper states, respectively to achieve our target $\tilde{\nu}_{if}$ limit of 8000 cm^{-1}. The recently developed GAIN (GPU Accelerated INtensities) code was utilized to compute 1,487,073,009 transitions within 6 h by exploiting M2090 nVidia

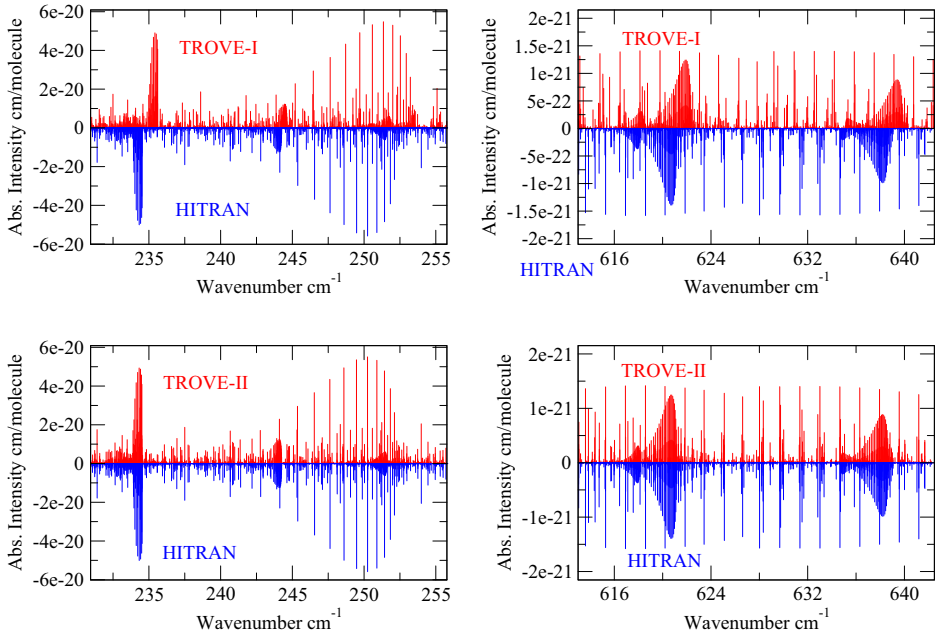

Fig. 8. Comparing two versions of the synthetic spectrum against HITRAN at T = 295 K. TROVE-I is the *ab initio*, TROVE-II is using the empirical band-center shifts.

graphics processing units (GPU) for their high degree of parallelism and computational efficiency. A paper discussing the methodology in detail will be published elsewhere [43].

3. Results

Using our line-list we obtained the partition function of 9840.91 at 296 K, which compares well to the HITRAN value 9819.80 [44].

Fig. 4 is our synthetic spectrum at 296 K for all 1.4 billion lines and comparing against the 126,983 lines from HITRAN highlights the significant degree of completeness our line-list provides. However two regions (1) and (2) show disagreement in line intensity, which can be attributed to the lack of the experimental data used for producing the HITRAN intensities by Perrin et al. [13,14].

The PNNL-IR [45] database provides additional cross-sections above 1800 cm^{-1}. Fig. 5 compares ours and HITRAN's simulated cross-sections to PNNL using a Gaussian convolution with HWHM at 0.312 cm^{-1} at $T = 323.15$ K and demonstrates that we agree much better in intensity and structure indicating problems with HITRAN intensities for these two regions.

Fig. 6 highlights a band in the 3.5 μm region which is a combination of the $(\nu_3 + 6\nu_4, \tau = 1) \leftarrow (0, \tau = 1)$, $(2\nu_3 + 4\nu_4, \tau = 1) \leftarrow (0, \tau = 1)$, $(3\nu_3, \tau = 1) \leftarrow (0, \tau = 2)$, $(\nu_3 + \nu_4 + \nu_5, \tau = 2) \leftarrow (0, \tau = 2)$, $(\nu_3 + 4\nu_4, \tau = 4) \leftarrow (0, \tau = 3)$ and other weaker hot bands. Good agreement is seen in both structure and overall intensity but our assumed Gaussian line profile utilized in our convolution may not be adequate enough to properly replicate the PNNL-IR cross-section leading to some minor differences in the overall cross-section.

Fig. 7 further illustrates the quality of both our line-positions and absolute intensities by comparing the ν_1 and ν_5 (ours vs PNNL-IR's) bands in the 2.7 μm region. As this is the region of most contention in the literature, it is to be hoped that this line-list may provide a means with which to assign the confusing spectra in this region.

Finally, the importance of the band shifts previously discussed is illustrated in Fig. 8. Here the TROVE-I spectra is purely using the *ab initio* band centers while TROVE-II utilizes the experimental band centers from Table 1. The *ab initio* deviation of 1.12 cm^{-1} reduces significantly to 0.005 cm^{-1} using this empirical shifting method.

4. Conclusions

Presented here is a high-quality room temperature line-list for H_2O_2 that covers the region up to 8000 cm^{-1}. The complete line-list is available at Exomol website: http://www.exomol.com. The ultimate goal is a hot line-list for H_2O_2 that reaches up to 10,000 cm^{-1}. Whilst there is extremely good agreement in both line-positions and intensities, the current strategy is to refine this PES to give a new spectroscopically-determined PES. The band-center shifting does resolve many discrepancies between the theoretical and experimental energy, however, due to the lack of line-positions, it may be not as accurate in predicting the nature of the ν_1 and ν_5 bands. By applying the refinement process, it may bring the PES closer to the 'true' form giving better predictions in this troublesome region. Nevertheless, this line-list can produce synthetic spectra that compare well with room temperature.

Acknowledgments

This work was supported by the ERC under the Advanced Investigator Project 267219 and made use of the DiRAC@Darwin, DiRAC@COSMOS HPC cluster and Emerald CfI cluster. DiRAC is the UK HPC facility for particle physics, astrophysics and cosmology and is supported by STFC and BIS. The authors would like to acknowledge the work presented here made use of the EMERALD High Performance Computing facility provided via the Centre for Innovation (CfI). The CfI is formed from the universities of Bristol, Oxford, Southampton and UCL in partnership with STFC Rutherford Appleton Laboratory. RIO thanks the Russian Fund for Fundamental Studies, Project 15-02-07887 A. AFA would also like to thank Dr. Faris N. Al-Refaie, Lamya Ali, Sarfraz Ahmed Aziz and Rory and Annie Gleeson for their support.

Appendix A. Supplementary data

Supplementary data associated with this article can be found, in the online version, at http://dx.doi.org/10.1016/j.jms.2015.10.004.

References

[1] D.D. Davis, Can. J. Chem. 52 (1974) 1405–1414.
[2] N.D.C. Allen, G.G. Abad, P.F. Bernath, C.D. Boone, J. Quant. Spectrosc. Radiat. Transf. 115 (2013) 66–77.
[3] K.V. Chance, D.G. Johnson, W.A. Traub, K.W. Jucks, Geophys. Res. Lett. 18 (1991) 1003–1006.
[4] S. Aoki, M. Giuranna, Y. Kasaba, H. Nakagawa, G. Sindoni, A. Geminale, V. Formisano, Icarus 245 (2015) 177–183.
[5] T. Encrenaz, B. Bezard, T.K. Greathouse, M.J. Richter, J.H. Lacy, S.K. Atreya, A.S. Wong, S. Lebonnois, F. Lefevre, F. Forget, Icarus 170 (2004) 424–429.
[6] T. Encrenaz, T.K. Greathouse, F. Lefevre, S.K. Atreya, Planet Space Sci. 68 (2012) 3–17.
[7] R.T. Clancy, B.J. Sandor, G.H. Moriarty-Schieven, Icarus 168 (2004) 116–121.
[8] P. Bergman, B. Parise, R. Liseau, B. Larsson, H. Olofsson, K.M. Menten, R. Güsten, Astron. Astrophys. 531 (2011) L8.
[9] K.P. Hand, M.E. Brown, Astrophys. J. Lett. 766 (2013) L21.
[10] R.H. Hunt, R.A. Leacock, C.W. Peters, K.T. Hecht, J. Chem. Phys. 42 (1965) 1931–1946.
[11] L.S. Rothman, I.E. Gordon, Y. Babikov, A. Barbe, D.C. Benner, P.F. Bernath, M. Birk, L. Bizzocchi, V. Boudon, L.R. Brown, A. Campargue, K. Chance, E.A. Cohen, L.H. Coudert, V.M. Devi, B.J. Drouin, A. Fayt, J.-M. Flaud, R.R. Gamache, J.J. Harrison, J.-M. Hartmann, C. Hill, J.T. Hodges, D. Jacquemart, A. Jolly, J. Lamouroux, R.J. Le Roy, G. Li, D.A. Long, O.M. Lyulin, C.J. Mackie, S.T. Massie, S. Mikhailenko, H.S.P. Müller, O.V. Naumenko, A.V. Nikitin, J. Orphal, V. Perevalov, A. Perrin, E.R. Polovtseva, C. Richard, M.A.H. Smith, E. Starikova, K. Sung, S. Tashkun, J. Tennyson, G.C. Toon, V.G. Tyuterev, G. Wagner, J. Quant. Spectrosc. Radiat. Transf. 130 (2013) 4–50.
[12] L.A. Zumwalt, P.A. Giguere, J. Chem. Phys. 9 (1941) 458–462.
[13] A. Perrin, J.-M. Flaud, C. CamyPeyret, R. Schermaul, M. Winnewisser, J.-Y. Mandin, V. Dana, M. Badaoui, J. Koput, J. Mol. Spectrosc. 176 (1996) 287–296.
[14] A. Perrin, A. Valentin, J.M. Flaud, C. Camy-Peyret, L. Schriver, A. Schriver, P. Arcas, J. Mol. Spectrosc. 171 (1995) 358–373.
[15] W.B. Olson, R.H. Hunt, B.W. Young, A.G. Maki, J.W. Brault, J. Mol. Spectrosc. 127 (1988) 12–34.
[16] C. Camy-Peyret, J.-M. Flaud, J.W.C. Johns, M. Noel, J. Mol. Spectrosc. 155 (1992) 84–104.
[17] P.A. Giguere, T.K.K. Srinivasan, J. Raman Spectrosc. 2 (1974) 125–132.
[18] G. Rauhut, G. Knizia, H.-J. Werner, J. Chem. Phys. 130 (2009) 054105.
[19] S.N. Yurchenko, W. Thiel, P. Jensen, J. Mol. Spectrosc. 245 (2007) 126–140.
[20] A. Yachmenev, S.N. Yurchenko, J. Chem. Phys. 143 (2015).
[21] P. Małyszekk, J. Koput, J. Comput. Chem. 34 (2013) 337–345.
[22] O.L. Polyansky, I.N. Kozin, P. Małyszek, J. Koput, J. Tennyson, S.N. Yurchenko, J. Phys. Chem. A 117 (2013) 7367–7377.
[23] S.N. Yurchenko, J. Tennyson, Mon. Not. R. Astron. Soc. 440 (2014) 1649–1661.
[24] C. Sousa-Silva, A.F. Al-Refaie, J. Tennyson, S.N. Yurchenko, Mon. Not. R. Astron. Soc. 446 (2015) 2337–2347.
[25] A.F. Al-Refaie, S.N. Yurchenko, A. Yachmenev, J. Tennyson, Mon. Not. R. Astron. Soc. 448 (2015) 1704–1714.
[26] C. Sousa-Silva, S.N. Yurchenko, J. Tennyson, J. Mol. Spectrosc. 288 (2013) 28–37.
[27] D.S. Underwood, J. Tennyson, S.N. Yurchenko, Phys. Chem. Chem. Phys. 15 (2013) 10118–10125.
[28] S.N. Yurchenko, A. Yachmenev, W. Thiel, O. Baum, T.F. Giesen, V.V. Melnikov, P. Jensen, J. Mol. Spectrosc. 257 (2009) 57–65.
[29] A. Yachmenev, S.N. Yurchenko, P. Jensen, O. Baum, T.F. Giesen, W. Thiel, Phys. Chem. Chem. Phys. 12 (2010) 8387–8397.
[30] I.N. Kozin, M.M. Law, J. Tennyson, J.M. Hutson, Comput. Phys. Commun. 163 (2004) 117–131.
[31] B.V. Noumerov, Mon. Not. R. Astron. Soc. 84 (1924) 592–602.
[32] J.W. Cooley, Math. Comp. 15 (1961) 363–374.
[33] P.R. Bunker, P. Jensen, Molecular Symmetry and Spectroscopy, second ed., NRC Research Press, Ottawa, 1998.
[34] S.N. Yurchenko, R.J. Barber, A. Yachmenev, W. Thiel, P. Jensen, J. Tennyson, J. Phys. Chem. A 113 (2009) 11845–11855.
[35] J.T. Hougen, Can. J. Phys. 62 (1984) 1392–1402.

[36] J.-M. Flaud, C. Camy-Peyret, J.W.C. Johns, B. Carli, J. Chem. Phys. 91 (1989) 1504–1510.
[37] A. Perrin, J.-M. Flaud, C. Camy-Peyret, A. Goldman, F.J. Murcray, R.D. Blatherwick, J. Mol. Spectrosc. 142 (1990) 129–147.
[38] R.J. Bartlett, M. Musiał, Rev. Mod. Phys. 79 (2007) 291–352.
[39] H.-J. Werner, P.J. Knowles, G. Knizia, F.R. Manby, M. Schütz, WIREs Comput. Mol. Sci. 2 (2012) 242–253.
[40] S.N. Yurchenko, in: Chemical Modelling, vol. 10, The Royal Society of Chemistry, 2014, pp. 183–228.
[41] E. Cohen, H. Pickett, J. Mol. Spectrosc. 87 (1981) 582–583.
[42] S.N. Yurchenko, W. Thiel, M. Carvajal, H. Lin, P. Jensen, Adv. Quant. Chem. 48 (2005) 209–238.
[43] A.F. Al-Refaie, J. Tennyson, S.N. Yurchenko, Comput. Phys. Commun. (2015) (submitted for publication).
[44] J. Fischer, R.R. Gamache, A. Goldman, L.S. Rothman, A. Perrin, J. Quant. Spectrosc. Radiat. Transf. 82 (2003) 401–412.
[45] S.W. Sharpe, T.J. Johnson, R.L. Sams, P.M. Chu, G.C. Rhoderick, P.A. Johnson, Appl. Spectrosc. 58 (2004) 1452–1461.